RSC Advances

This is an *Accepted Manuscript*, which has been through the Royal Society of Chemistry peer review process and has been accepted for publication.

Accepted Manuscripts are published online shortly after acceptance, before technical editing, formatting and proof reading. Using this free service, authors can make their results available to the community, in citable form, before we publish the edited article. This *Accepted Manuscript* will be replaced by the edited, formatted and paginated article as soon as this is available.

You can find more information about *Accepted Manuscripts* in the Information for Authors.

Please note that technical editing may introduce minor changes to the text and/or graphics, which may alter content. The journal's standard Terms & Conditions and the Ethical guidelines still apply. In no event shall the Royal Society of Chemistry be held responsible for any errors or omissions in this *Accepted Manuscript* or any consequences arising from the use of any information it contains.

ROYAL SOCIETY OF CHEMISTRY

www.rsc.org/advances

A superparamagnetic and well - dispersed nanocomposite has been successfully synthesized by *in situ* polymerization method using the hollow $Ni_{0.3}Zn_{0.5}Fe_2O_4$ nanoparticles (h-NZFO) as fillers and the waterborne polyurethane (WPU) as matrix. The h-NZFO nanoparticles modified by chemical method would combine with the WPU prepolymer through covalent bond instead of simple mechanical mixing. The results indicated that the functionalized h-NZFO nanoparticles were wrapped and dispersed homogeneously in the WPU matrix. The introduction of functionalized h-NZFO contributed to thermal stability, the glass transition temperature, emulsion stability etc. Furthermore, the nanocomposite films present superior magnetic properties and the maximum saturation magnetization reached up to 15.24 emu cm^{-3}, which would have a promising application in microwave - absorption field.

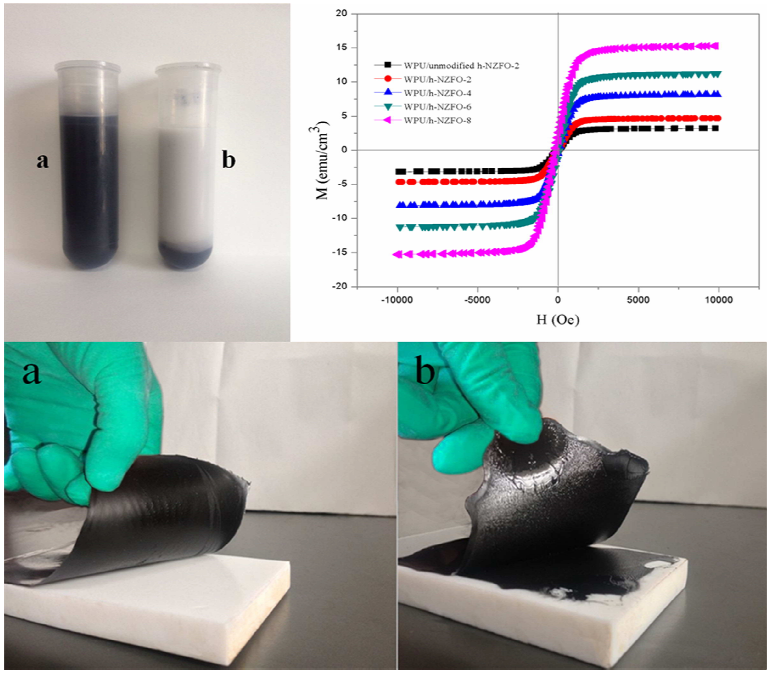

RSC Advances Accepted Manuscript

Fabrication and properties of superparamagnetic UV-curable nanocomposites based on covalently linked waterborne polyurethane/functionalized hollow $Ni_{0.3}Zn_{0.5}Fe_2O_4$ microspheres

Suli Chen, Wenling Wu, Guanghui Zhao*, Tao Jin, Tianqi Zhao

State Key Laboratory of Applied Organic Chemistry, Key Laboratory of Nonferrous Metal Chemistry and Resources Utilization of Gansu Province, College of Chemistry and Chemical Engineering, Institute of Biochemical Engineering and Environmental Technology, Lanzhou University, Lanzhou, 730000, China

The UV-curable nanocomposites based on waterborne polyurethane (WPU)/hollow $Ni_{0.3}Zn_{0.5}Fe_2O_4$ nanospheres (h-NZFO) have been successfully synthesized by *in situ* polymerization method. The h-NZFO nanoparticles prepared by solvothermal method were modified with isophorone diisocyanate (IPDI) via chemical method to improve the compatibility with monomers. The functionalized hollow - $Ni_{0.3}Zn_{0.5}Fe_2O_4$ fillers (h-NZFO-NCO) acted as an efficient crosslinker in prepolymer and combined with waterborne polyurethane by chemical bond instead of the conventional physical mixing. It was found that the h-NZFO-NCO nanoparticles were wrapped and dispersed homogeneously in the WPU matrix. Moreover, the introduction of h-NZFO-NCO obviously contributed to thermal stability, glass transition temperature (T_g), emulsion stability and the magnetic properties of WPU/h-NZFO nanocomposite. The saturation magnetization of nanocomposites can reach up to 15.24 emu cm^{-3} with h-NZFO-NCO doping is 8%, which would have the potential application in microwave - absorbing field.

1. Introduction

RSC Advances Accepted Manuscript

Recently, the inorganic - organic nanocomposites have been widely studied and drawn increasing attention in many fields. [1-4] In particular, the system that inorganic nanoparticles acted as fillers in different polymer matrixs has attracted great interest, because it could offer some specific advantages, such as improved properties of polymer, made up for defects of polymer and obtained functional nanocomposite materials. In this context, oxides like SiO_2, TiO_2, Fe_3O_4, Al_2O_3 etc., [5-8] carbon material like carbon nanotube, graphene, [9, 10] metal particles like Au and Ag, [11, 12] silicate like attapulgite, montmorillonite etc., [13, 14] were usually used as fillers in different polymer matrix to investigate.

Waterborne polyurethane (WPU) is a new type of polyurethane system using water as solvent instead of the organic solvents and widely used in membranes, coatings, and biological fields. [15, 16] Therefore, it could make a great contribution to the environment protection by reducing the release of volatile organic compounds (VOC). Furthermore, the WPU presents attractive characteristics of superior process ability, high film-forming ability, excellent elasticity of its membranes and non-toxicity compared with conventional PUs. [17] Thus, the WPU turns into a satisfying polymer matrix with the advantages and is used in various industrial fields. In the WPU preparation process, isophorone diisocyanate (IPDI) is a preferable reaction monomer to prepare WPU polymer. Because compared to other aromatic isocyanates, IPDI shows higher weather resistance, better controllable activity and more rigidity contribution to polymers. [18, 19] However, the development and application of WPU were limited by the low thermal stability, poor mechanical properties etc. To date, in

RSC Advances Accepted Manuscript

order to solve this issue, some measures have been taken, for example, adding inorganic particles, increasing crosslink of density etc. In previous works, different kinds of inorganic particles have been added to WPU matrix to form composites, [20, 21] however, on one hand, the nanoparticles can easily aggregate and not be homogeneously dispersed in matrix when the inorganic fillers mixed with polymer matrix by simple mechanical mixing, this has a negative influence on properties of the resulting nanocomposites. On the other hand, the fillers are generally used to enhance the mechanical properties of polymers without other functional groups.

The $Ni_{0.3}Zn_{0.5}Fe_2O_4$ (Ni-Zn ferrite) is a kind of spinel ferrite and has been intensively investigated due to the high Curie temperature, high resistivity, low dielectric losses and excellent microwave - absorbing properties. [22] Meanwhile, the Ni-Zn ferrite became a favorable of material filler in polymer because of the excellent magnetic properties, good mechanical abrasion resistance and chemical stability. Adding Ni-Zn ferrite in polymer matrix not only makes up for the defects of polymer but also endows polymer with magnetic properties, and the nanocomposites have wide application in many fields, such as microwave - absorbing field, power transformers in electronics and electromagnetic interference (EMI). [23- 25] To the best of our knowledge, there are fewer papers studied the magnetic properties of nanocomposite based on WPU and hollow Ni-Zn ferrite so far. The final WPU/h-NZFO nanocomposites with excellent magnetic properties would have a wide application in microwave absorption. [26] Moreover, Ni-Zn ferrite with hollow structure has lower density than solid Ni-Zn ferrite, which is very significant when

RSC Advances Accepted Manuscript

WPU/h-NZFO nanocomposites are used as microwave absorbers.

In this study, the modified h-NZFO was used to blend with WPU to obtain WPU/h-NZFO nanocomposites with magnetic properties and improve performances of WPU. Both the h-NZFO-NCO and WPU prepolymer contained plenty of isophorone diisocyanate groups (-NCO) which could react with trimethylolpropane (TMP). Therefore, the h-NZFO-NCO fillers could be combined with WPU by chemical bond. In addition, the h-NZFO-NCO also acted as an effective crosslink point which would contribute to improvement of density of cross-linking and better physical properties of nanocomposites.

2. Experimental

2.1. Materials

Ferric chloride hexahydrate ($FeCl_3 \cdot 6H_2O$), trimethylolpropane (TMP) and poly (propylene glycol) (PPG-2000) were purchased from Sinopharm Chemical Reagent Co., Ltd (China). Zinc chloride ($ZnCl_2$), ammonium acetate (NH_4Ac) and triethylamine (TEA) were supplied by Tianjin Guangfu Technology Development Co.LTD (China). Nickel chloride hexahydrate ($NiCl_2 \cdot 6H_2O$) was purchased from Tianjin Kermel Chemical Reagent Co., Ltd (China). Poly (propylene glycol) (PEG-6000) was obtained from Tianjin Tiantai Fine Chemical Co., Ltd (China). Ethylene glycol and isophorone diisocyanate (IPDI) were purchased from Shanghai Chemical Reagents Corp. (China). Hydroxyethyl methacrylate (HEMA) was purchased from Tianjin Institute of chemical reagents (China). Dibutyltin diaurate (DBTDL) and dimethylol propionic acid (DMPA) were obtained from Aldrich

RSC Advances Accepted Manuscript

Chemical (China) and dried in vacuum for 24 h at 80 °C. Irgacure 2959 as photoinitiator was obtained from Sigma-Aldrich Co. Toluene and acetone are dehydrated via 4Å MS before use. All reagents are of analytical purity.

2.2. Preparation of hollow $Ni_{0.3}Zn_{0.5}Fe_2O_4$ (h-NZFO) nanoparticles

The h-NZFO nanoparticles were prepared through a solvothermal method according to our previous work. [27] 1.08 g of $FeCl_3 \cdot 6H_2O$, 0.19 g of $ZnCl_2$, 0.14 g of $NiCl_2 \cdot 6H_2O$, 7.71 g of NH_4Ac and 6.30 g of PEG-6000 were dissolved in 70 mL ethylene glycol and stirred vigorously until homogeneous dispersion, and then the solution was transferred to a Teflon-lined autoclave and was calcined in a silicon carbide furnace at 200 °C for 12 h. Removing the supernatant of the resulting solution and washing with ethanol and distilled water by magnetic decantation in sequence. Finally, the black product was obtained and dried in vacuum for 12 h at 40 °C.

2.3. Chemical modification of h-NZFO nanoparticles

0.10 g of h-NZFO particles and 40 mL toluene were added in a flask equipped with a mechanical stirring, a nitrogen gas inlet and a condenser with a $CaCl_2$ drying tube firstly under ultrasonic. Subsequently, a certain amount of IPDI was added under mechanical stirring and kept ultrasonic continuously for 0.5 h. 5~6 drops of DBTDL was added and heated up to 110°C, refluxing for 24 h in toluene. Lastly, the resulting product was washed with toluene and acetone by ultrasonication, drying in vacuum for 24 h at 40 °C, the h-NZFO-NCO was obtained.

2.4. Synthesis of WPU/h-NZFO nanocomposites

The procedure was briefly described as follows: 0.67 g of DMPA, 10.00 g of

RSC Advances Accepted Manuscript

PPG-2000 and 5.00 g of acetone were put into a flask firstly under N_2 protection and mechanical stirring to form a homogenous system. Subsequently, 4.45 g of IPDI and a few drops of DBTDL were introduced to the reactor, refluxing for 3 h at 80 °C. 2.60 g of HEMA was added to solution after cooling to 60 °C and reacted for 2 h. Later, cooling to room temperature and adding different stoichiometric h-NZFO-NCO to system by ultrasonic treatment for 1 h. Subsequently, 0.13 g TMP was added and reacted for another 2 h at 60 °C. Then the mixture was neutralized by the addition of TEA and stirred at 40 °C for 30 min. A suitable amount of acetone could add to adjust the system viscosity during above preparation process. At last, the mixture was emulsified by adding distilled water slowly to the system and stirring vigorously for another 0.5 h to form homogenous WPU/h-NZFO dispersions. The final dispersions had 30% solid contents after removing acetone via spin steaming.

2.5. Film preparation

The latex film of WPU/h-NZFO was prepared by the mixing of preweighted nanocomposite emulsion and 3 wt% of Irgacure 2959 firstly, followed by rapid stirring to form a homogeneous emulsion. Subsequently, the mixed emulsion was spread on a clean Teflon plate surface and dried for 8 h at room temperature to remove most of the water before curing. Lastly, the sample was exposed under ultraviolet light (medium-pressure mercury lamp, 1000 W, wavelength of 295 nm) to cure for 4 min, then the final product was obtained. The distance between UV-lamp and film sample is 40 cm. Additionally, the nanocomposite films prepared in this paper with h-NZFO-NCO mass fraction of 0, 2%, 4%, 6% and 8% are marked as

RSC Advances Accepted Manuscript

WPU, WPU/h-NZFO-2, WPU/h-NZFO-4, WPU/h-NZFO-6, and WPU/h-NZFO-8, respectively. The synthesis scheme of WPU/h-NZFO film is shown in Fig. 1. What's more, in the reaction system, the composition of the resulting film samples was controlled by many factors, such as reaction condition, reactant proportion, reaction temperature and time. IPDI, PPG-2000, HEMA etc. were added according to specific stoichiometric ratio, and reaction temperature and time were controlled, which can made great contribution to the polymer structure in Fig. 1, especially made HEMA is mainly encapped in one end of the polymers.

2.6. Characterization

The morphology and microstructure of the samples were investigated using scanning electron microscope (SEM, JSM-6380Lv, JEOL, Japan; JSM-6701F, JEOL, Japan) and transmission electron microscopy (TEM, FEI Tecnai G20). Power X-ray diffraction (XRD, Rigaku D/MAX-2400 X-ray diffractometer with Ni-filtered Cu Kα radiation) was used to identify the crystal structure of nanoparticles. Fourier transform infrared (FT-IR) spectra were obtained by means of an infrared spectrophotometer (American Nicolet Corp. Model 170-SX) utilizing KBr pellets technique. TGA of nanocomposite samples were conducted with a thermogravimetric analyzer from TA Instrument (NETZSCH STA 449C) under a stable N_2 flow with the temperature ranging from room temperature to 800 °C. Dynamic mechanical thermal analysis (DMTA, Mettler-Toledo) was performed from -30 to 200 °C at the heating rate of 5 °C/min. The magnetic properties of products were measured by vibrating sample magnetometer (VSM, LAKESHORE-7304, USA) at room temperature. The tensile

RSC Advances Accepted Manuscript

properties of nanocomposite films were investigated by drawing machine according to the national standard GBI447-83 with the drawing speed of 30 mm/min. The particle size and size distribution of emulsions was measured by a dynamic light scattering (DLS) (Zeta-plus, Brookehaven Instruments). The samples for DLS test were diluted in deionized water to 0.5%, then kept ultrasonic to form homogenous dispersions.

3. Results and discussion

3.1. Morphology and structure of h-NZFO and WPU/h-NZFO nanocomposites

The morphology of h-NZFO and nanocomposites were characterized by TEM and SEM. Fig. 2(a) shows the TEM image of h-NZFO particles, the particles are hollow spherical and with the diameter ranging from 240 to 300 nm. Fig. 2(b)-(f) show the SEM micrographs of cross-section of film products. The pure WPU in Fig. 2(b) shows a smooth and glassy surface. Fig. 2(c) and (d) are SEM micrographs of nanocomposites with the original h-NZFO and h-NZFO-NCO mass fraction is 4%, respectively. Compared with pure WPU, the fracture surfaces of WPU/h-NZFO nanocomposites become much rougher. Fig. 2(d) presents better dispersion than Fig. 2(c) and the h-NZFO-NCO nanoparticles are well wrapped and homogeneously dispersed in WPU matrix, which indicated that functionalized h-NZFO is well adhered to the WPU matrix. Fig. 2(e) exhibits SEM image of nanocomposite with h-NZFO-NCO content is 6%, it is observed that there is less reunion occurred in the nanocomposites, but overall, the h-NZFO-NCO nanoparticles are still evenly dispersed in WPU matrix. However, it was observed from Fig. 2(f) that the h-NZFO-NCO nanoparticles begin to aggregate seriously when the h-NZFO-NCO

RSC Advances Accepted Manuscript

content increases to 8%. Uniform distribution of ferrite nanoparticles in matrix would contribute to physical properties of the final nanocomposite films. [28]

The crystal structure of h-NZFO nanoparticle is investigated by X-ray diffraction. Fig. 3(a) presents the XRD pattern of h-NZFO. Several obvious diffraction peaks are observed at $2\theta = 18.3^{\circ}$, 30.1°, 35.4°, 43.1°, 53.4°, 56.9°, 62.5°, which are assigned to the (111), (220), (311), (400), (422), (511), (440) planes. The diffraction peaks of h-NZFO-NCO in Fig. 3(b) become weaker than original h-NZFO because the interaction has formed between IPDI and h-NZFO. This proved that the crystal structure of h-NZFO hasn't been changed after being modified. It can be seen from Fig 3(c) and d that a broad scatting peak appeared between 15° and 26°, which results from orderly arrangement of soft segments of WPU. [29]

To further identify the structures of h-NZFO-NCO and WPU/h-NZFO nanocomposite, fourier transform infrared spectroscopy was conducted. The FT-IR spectra are shown in Fig. 4. The characteristic peak at 578 cm^{-1} is mainly attributed to stretching vibration of Fe-O bond, which has been observed in figure 4(a) (h-NZFO), (b)(h-NZFO-NCO) and (e)(WPU/h-NZFO-4). Due to low content of h-NZFO in WPU nanocomposites, a relatively weak peak at 578 cm^{-1} occurred in WPU/h-NZFO-4 nanocomposite. Compared with h-NZFO, the peak of h-NZFO-NCO in Fig. 4(b) at about 2270 cm^{-1} is the characteristic absorption of isocyanate group. [30, 31] Furthermore, several new peaks occurred at 3405, 1427 and 1258 cm^{-1} in h-NZFO-NCO, which are the stretching vibration absorption peaks of newly formed -N-H, -C-N and C-O bonds resulting from the reaction between -NCO and -OH

RSC Advances Accepted Manuscript

groups. In addition, the newly formed peak at 1560 and 1650 cm^{-1} are attributed to the blending vibration of -N-H and stretching vibration of -C=O, respectively. [13] As can be seen, the peaks in other samples at 1560 and 1710 cm^{-1} are attributed to the blending vibration of -N-H and stretching vibration of -C=O, respectively. The characteristic peaks of $-CH_2$, $-CH_3$ and -CH at 2950 and 2850 cm^{-1} are clearly observed in h-NZFO-NCO, pure WPU, and WPU/h-NZFO-4. Compared to the h-NZFO-NCO and pure WPU, on one hand, the peak at 2270 cm^{-1} of -NCO disappeared in WPU/h-NZFO-4 nanocomposite, implied that -NCO groups have participated in reaction. Moreover, the absorption of C=O at 1710 cm^{-1} is enhanced significantly. And on the other hand, the peak at 578 cm^{-1} of Fe-O can be also observed clearly in nanocomposites. All of above analysis indicated that the -NCO was successfully grafted on the h-NZFO surface and WPU/h-NZFO nanocomposite was obtained.

The particle size and size distribution of pure WPU and WPU/h-NZFO-4 emulsions were measured by DLS as shown in Fig. 5. It's was observed that the average size particle of pure WPU (Fig. 5(a)) was only 87.8 nm with very narrow distribution width, however, the average size of WPU/h-NZFO-4 (Fig. 5(b)) increased to about 311 nm, which has a great effect on emulsion stability, as we'll discuss later. Furthermore, the morphology of emulsion samples were also characterized by TEM and were presented in Fig. 6. Fig. 6(a) was the TEM image of pure WPU emulsion, it can be seen that the WPU particles were well dispersed. Fig. 6(b) displayed the TEM image of WPU/h-NZFO-4 emulsion. Compared to pure WPU, the size particle

RSC Advances Accepted Manuscript

increased when the h-NZFO-NCO was introduced to the system, and the result was in accordance with above DLS analysis. We can see from Fig. 2(a) that the diameter of pure h-NZFO particles were ranged from 240 to 300 nm. This indicated that the h-NZFO-NCO particles were effectively compounded with WPU matrix, leading to the increasing of size particles.

3.2. Thermal analysis of WPU/h-NZFO nanocomposites

Thermogravimetric analysis (TGA) was carried out to investigate the effect of h-NZFO-NCO content on the thermal stability of WPU/h-NZFO films. Fig. 7 shows typical TGA curves for WPU/h-NZFO nanocomposites. It is observed that the h-NZFO-NCO nanoparticles has a great effect on thermal stability of nanocomposites. According to Fig. 7, the thermal stability of nanocomposites is far superior to pure WPU and all the samples exhibit three distinct weight loss stages. The temperature for the first weight loss stage ranges from 25~250 °C, results from the evaporation of residual water and the unreacted organic molecular in the WPU and nanocomposites. The second weight loss stage exhibits in the range of 250~395 °C and the thermal decomposition temperature range in third stage is between 269 and 394 °C. The second stage is possibly due to the decomposition of the hard segment. The third stage might be assigned to the decomposition of the later decomposition of the soft segment of WPU. [32, 33] The results revealed that the introduction of h-NZFO-NCO obviously improve the initial degradation temperature of WPU. The initial degradation temperature of nanocomposites shifts toward the higher temperature than pure WPU, increases from 268 °C for pure WPU to 298 °C for WPU/h-NZFO-8, which is higher

RSC Advances Accepted Manuscript

than the work we reported previously. [34, 35] It is observed from TGA curves that h-NZFO-NCO fillers remarkably boost the thermal stability of nanocomposites as the h-NZFO-NCO content increases. The reasons might be explained as following: firstly, the existence of inorganic oxides would endow the nanocomposites better stability at high temperature. Secondly, the strong interaction between h-NZFO and WPU formed through TMP, because TMP acted as cross-linking agent can react with -NCO group on both h-NZFO-NCO surface and -NCO terminated polyurethane simultaneously. Moreover, hydrogen bond also formed between h-NZFO-NCO and WPU chain as well as WPU chains (-NH and -C=O), they work together to enhance the interaction between the organic and inorganic two-phase to improve the dispersion of h-NZFO in the WPU matrix. [13] In addition, the addition of TMP leads to the increase of cross-link density, this is another reason for the improvement of thermal stability. Meanwhile, the degradation rate of polymer was reduced by the addition of h-NZFO-NCO at lower temperature area with temperature ranging from 100 to 350 °C, and later increased with the h-NZFO-NCO loading increased after 350 °C. This phenomenon may be explained by the improvement of cross-linking degree, the higher degree of cross-linking, the slower membrane degradation rate. However, as the temperatures continue to rise and higher 350 °C, the degradation rate turned to increased with h-NZFO-NCO loading increased, this is because h-NZFO-NCO as metal oxide which catalyzed the degradation of the polymer at higher temperature.

The viscoelastic properties of WPU/h-NZFO films were investigated by DMTA. And loss factor (tan δ) and the storage modulus (E′) curves are shown in Fig. 8 and 9.

RSC Advances Accepted Manuscript

The glass transition temperature (T_g) is obtained from tan δ curve (Fig. 8). It is observed that T_g value of pure WPU is 42.3 °C and increases to 66.5, 77.8 and 98 °C for WPU/h-NZFO-2, WPU/h-NZFO-4, WPU/h-NZFO-6, respectively. The increased content of h-NZFO-NCO enhances the stiffness of the nanocomposites and has a obvious favorable influence on Tg. What is more, the Tg value is higher than the data of 78 °C reported in our previous work, [34] this could be attributed to the strong interaction between inorganic phase and organic phase and improvement of cross-link density. As can be seen from Fig. 9, storage modulus also increases as h-NZFO-NCO content increases, we can explain this as follows: storage modulus is relevant to the interfacial interaction and the cross-linking density of the polymer, and h-NZFO-NCO acted as an effective crosslink point increases the cross-linking density of WPU. Meanwhile, and the interfacial interaction does not deteriorate the storage modulus, even though it is poor, therefore, the introduction of h-NZFO-NCO contributed to the improvement of E′. However, both T_g and E′ decreased when the h-NZFO-NCO content reaches 8%, which is due to the decrease of the cross-link density resulted from aggregation of h-NZFO-NCO nanoparticles. The h-NZFO-NCO nanoparticles tended to aggregate at high content and resulted in increasing system heterogeneity, which led to a decrease in T_g and E′. This is consistent with above SEM analysis.

3.3. Emulsion stability of nanocomposites

The emulsion stability was conducted by placing composite emulsions with different h-NZFO-NCO loading at room temperature for a certain time. And the longer stable time, the better stability. The result was shown in Table 1. What's more,

RSC Advances Accepted Manuscript

Fig. 9 also provided the picture of nanocomposite emulsion of WPU/h-NZFO-4 and WPU/pristine h-NZFO-4. It demonstrated that h-NZFO-NCO had a great effect on emulsion stability. From Table 1 and Fig. 10, the emulsion of WPU/h-NZFO-4 still contained a uniform system until placing after one month (Fig. 10(a)), while obvious stratification phenomenon occurred in the emulsion of WPU/pristine h-NZFO-4 after placing for less than half an hour (Fig. 10(b)). The reason may be ascribed to phase separation. Because the pristine h-NZFO combined with WPU polymer through simple mechanical mixing, there is no interaction formed between inorganic and organic phase. This made most of h-NZFO particles mainly exist in water phase, they can't be wrapped in the WPU matrix, thereby inorganic nanoparticles are precipitated off gradually from the system. Above phenomenon demonstrated that the functionalized h-NZFO made a great contribution to improving the emulsion stability of nanocomposites, and the result should be attributed to the strong interaction (covalent bonds and hydrogen bonds) between the h-NZFO-NCO and WPU matrix. Additionally, the stability was obviously declined when the h-NZFO-NCO loading was up to 6%, the stable time suddenly reduced to 24 days for WPU/h-NZFO-6 and 19 days for WPU/h-NZFO-8. This should be attributed to the aggregation phenomenon occurred in the nanocomposites (Fig. 2(e), (f)). In the nanocomposite emulsions with high inorganic nanoparticles content, the h-NZFO-NCO (especially unreactive particles) were more likely to gather together to form large aggregates, which was easily separated from the organic matrix system, leading to poor emulsion stability.

RSC Advances Accepted Manuscript

What's more, emulsion stability has a great effect on film-forming ability. Fig. 11 presents film-forming process of WPU/h-NZFO-4 and WPU/pristine h-NZFO-4 films, respectively. The WPU/h-NZFO-4 film can be peeled off easily, obtaining a nanocomposite film with smooth surface (Fig. 11(a)), however, the WPU/pristine h-NZFO-4 film can't be completely peeled off, leaving part of composites on a Teflon plate surface (Fig. 11(b)), and obtain a broken film, which would have a negative effect on performances of final nanocomposites. As illustrated above, the result should be ascribed to poor emulsion stability of WPU/pristine h-NZFO-4 which led to the filler nanoparticles easily sank to the bottom, causing membrane delamination when peeling off. In order to further examine the composition difference of WPU/h-NZFO-4 and WPU/pristine h-NZFO-4, the SEM micrographs of surfaces of above two films were conducted and shown in Fig. 12. Fig. 12(a) and (b) are upper surface and lower surface of WPU/h-NZFO-4 film, respectively. It was observed that both upper and lower surface of WPU/h-NZFO-4 film are rough and h-NZFO-NCO particles were wrapped in the WPU matrix, there aren't any exposed particles on the film surface. Fig. 12(c) and (d) are upper surface and lower surface of WPU/pristine h-NZFO-4 film, respectively. Compared with WPU/h-NZFO-4, the upper surface of WPU/pristine h-NZFO-4 was glassy with little pristine h-NZFO on it, while there are a lot of agglomerated h-NZFO particles exposed on the lower surface of WPU/pristine h-NZFO-4. This further demonstrated that the poor emulsion stability really resulted in phase separation and led to weak film-forming ability.

3.4. Magnetic properties of WPU/h-NZFO nanocomposites

RSC Advances Accepted Manuscript

The hysteresis loops of pristine h-NZFO and h-NZFO-NCO are obtained from vibrating sample magnetometer at room temperature and are shown in Fig. 13(a). Coercive force (H_c) and remnant magnetization (M_r) are almost equal to zero, which reveals that h-NZFO exhibits a superparamagnetic behavior. The maximum saturation magnetization (Ms) of original h-NZFO is about 81.91 emu g^{-1}, and reduces to 74.21 emu g^{-1} after modification, which further indicated that the IPDI was successfully grafted to h-NZFO surface. Fig. 13(b) shows the hysteresis loops of nanocomposites with different h-NZFO-NCO content. It is clear that the maximum saturation magnetization of nanocomposites is less than h-NZFO nanoparticles. The functionalized h-NZFO made greater contribution to magnetic properties of nanocomposite films than pristine h-NZFO. The maximum saturation magnetization of WPU/h-NZFO-2% is 4.66 emu cm^{-3}, which is higher than WPU/pristine h-NZFO-2 (3.17 emu cm^{-3}). This may be attributed to the membrane delamination in preparation process resulted from the poor emulsion stability of WPU/pristine h-NZFO-2, because most of magnetic naoparticles precipitated and stayed in Teflon plate surface in film preparation process and can be observed from Fig. 11 and 12. Furthermore, the magnetism of nanocomposites are affected by nanoparticle size, surface disorder and distribution. [36] Herein, because h-NZFO-NCO nanoparticles combined with WPU matrix through covalent bonds, namely strong interaction have formed between inorganic particles and WPU, which improved the distribution of h-NZFO nanoparticles in the WPU matrix, resulting in the increase of magnetization of WPU/h-NZFO nanocomposites. The maximum saturation magnetization of

RSC Advances Accepted Manuscript

nanocomposites increases with the increase of h-NZFO-NCO content, reaching up to 15.24 emu/cm^3 when h-NZFO-NCO content is 8%. The maximum saturation magnetization is largely improved compared to the reported film products, [37, 38] and also higher than our reported work. [35] The results proved that the final nanocomposites presented superior magnetic properties, having extensive application prospect in microwave - absorbing field.

3.5. Mechanical properties of WPU and WPU/h-NZFO nanocomposites

The influences of h-NZFO content on mechanical properties of WPU/h-NZFO films are studied by using the computer controlled universal tensile testing machine. Table 2 shows the tensile strength, elongation at break and Young's modulus data of WPU and WPU/h-NZFO films. It was observed from Table 2, the pure WPU exhibits a nonlinear elastic behavior and has a low tensile strength of 17.5 MPa and a high elongation at break of about 386% because of its amorphous nature and the Young's modulus and elongation at break gradually decrease with the increase of h-NZFO content, this result is in agreement with some reported works. [13, 31, 34] The tensile strength increases firstly and reaches the maximum value of 19.50 MPa at 4%. The increases of tensile strength firstly may be attributed to strong chemical interaction formed between h-NZFO and WPU chains, which made a homogeneous dispersion of h-NZFO in WPU matrix. Moreover, the improvement of cross-linking density was also contributed to increase of tensile strength. However, as the loading of h-NZFO-CNO increases to 6%, the tensile strength of the nanocomposite decreases and higher h-NZFO-CNO loading (up to 8%) results in more serious decrease. On one

RSC Advances Accepted Manuscript

hand, higher h-NZFO content could cause serious aggregation of h-NZFO nanoparticles, which would easily lead to phase separation between h-NZFO nanoparticles and WPU, thereby causing the decease of the tensile strength. And on the other hand, because increased h-NZFO-NCO would lead to higher cross - linking density of nanocomposites. Excessive crosslink structure of polymers can result in the increasing particle size of WPU emulsion and WPU emulsion will be unstable due to the severe aggregation, which can be observed from Table 1 and Fig 10. Unstable WPU emulsion has a negative effect on the film-forming properties, which result in the decrease of tensile strength of final materials. Generally, the resistance to local deformation is related to the cross-linking density. However, with the increase of the h-NZFO-CNO content, the compatibility and phase structure of WPU matrices may become worse, so it can lead to phase separation between the WPU and h-NZFO-CNO nanoparticles and reduce their Young's modulus and the elongation at break ultimately.

4. Conclusions

A series of UV-curable magnetic WPU/h-NZFO nanocomposites were successfully prepared by *in situ* polymerization method. The h-NZFO nanoparticles were modified by chemical method and combined with the WPU through covalent bonds. The microstructure of nanocomposites could be seen clearly in SEM images and suggested that the functionalized h-NZFO nanoparticles were dispersed homogeneously in WPU matrix. The introduction of h-NZFO-NCO nanoparticles obviously improved thermal stability, glass transition temperature and emulsion stability of nanocomposites

RSC Advances Accepted Manuscript

compared with the pure WPU. Moreover, the WPU/h-NZFO nanocomposites had exhibited superior magnetic properties and the maximum saturation magnetization reached up to 15.24 emu cm^{-3}. In summary, this work synthesized a series of nanocomposites with good physical properties and excellent magnetic properties, which have a promising application in microwave - absorbing field.

Acknowledgments

The authors acknowledge financial supports from the National Training Fund for Talented Person of Basic Subjects ((J1103307) and the Opening Foundation of State Key Laboratory of Applied Organic Chemistry (SKLAOC-2009-35).

References

[1] X. Yuan, X. Zeng, H. J. Zhang, Z. F. Ma and C. Y. Wang, *J. Am. Chem. Soc.*, 2010, **132**, 1754-1755.

[2] J. Hu, L. Liu, Y. Xie and L. Wu, *Polym. Chem.*, 2013, **4**, 3293-3299.

[3] A. P. Bonifas and R. L. McCreery, *Anal. Chem.*, 2012, **84**, 2459-2465.

[4] J. Wu, X. Zhang, T. Yao, J. Li, H. Zhang, and B. Yang, *Langmuir*, 2010, **26**, 8751-8755.

[5] L. Zhang, H. Zhang and J. Guo, *Ind. Eng. Chem. Res.*, 2012, **51**, 8434-8441.

[6] G. Liao, S. Chen, X. Quan, H. Chen and Y. Zhang, *Environ. Sci. Technol.*, 2010, **44**, 3481-3485.

[7] W. Zhou, X. Hu, X. Bai, S. Zhou, C. Sun, J. Yan and P. Chen, *ACS. Appl. Mater. Inter.*, 2011, **3**, 3839-3845.

[8] S. A. Suthanthiraraj and D. J. Sheeba, *Ionics.*, 2007, **13**, 447-450.

RSC Advances Accepted Manuscript

[9] Z. Spitalsky, D. Tasis, K., Papagelis and C. Galiotis, *Prog. Polym. Sci.*, 2010, **35**, 357-401.

[10] K. Zhang, L. L. Zhang, X. S. Zhao and J. Wu, *Chem. Mater.*, 2010, **22**, 1392-1401.

[11] S. Liu, H. Xu, J. Ou, Z. Li, S. Yang and J. Wang, *Mater. Chem. Phys.*, 2012, **132**, 500-504

[12] M. Jouni, A. Boudenne, G. Boiteux, V. Massardier, B. Garnier and A. Serghei, *Polym. Composites.*, 2013, **34**, 778-786.

[13] L. Peng, L. Zhou, Y. Li, F. Pan and S. Zhang, *Compos. Sci. Technol.*, 2011, **71**, 1280-1285.

[14] G. S. Venkatesh, A. Deb, A. Karmarkar and S. S. Chauhan, *Mater. Design.*, 2012, **37**, 285-291.

[15] I. S. Gunes, F. Cao and S. C. Jana, *Polym.*, 2008, **49**, 2223-2234.

[16] M. Yu, S. H. Chen, Z. Zhou and M. F. Zhu, *Prog. Nat. Sci - Mater.*, 2012, **22**, 288-294.

[17] J. J. Chen, C. F. Zhu, H. T. Deng, Z. N. Qin and Y. Q. Bai, *J. Polym. Res.*, 2009, **16**, 375-80.

[18] G. Grüll, R. Fitl and A. Teischinger, *Surf. Coat. Int. Part B: Coat. Trans.*, 2006, **89**, 99-107.

[19] C. Saha, T. K. Chaki, Chaki and N. K. Singha, *J. Appl. Polym. Sci.*, 2013, **130**, 3328-3334.

[20] S. Zhou, B. Zhou, C. Y. Huang and J. J. Chen, *Adv. Mater. Res.*, 2013, **668**,

RSC Advances Accepted Manuscript

388-392.

[21] D. Wu, H. Xu, F. Qiu and D. Yang, *Polym - Plast. Technol.*, 2011, **50**, 498-508.

[22] P. Gao, E. V. Rebrov, T. M. Verhoeven, J. C. Schouten, R. Kleismit, G. Kozlowski, ... and G. Subramanyam, *J. Appl. Phys.*, 2010, **107**, 044317.

[23] K. Shimba, N. Tezuka and S. Sugimoto, *Mater. Sci. Eng. B*, 2012, **177**, 251-256.

[24] A. C. F. M. Costa, E. Tortella, M. R. Morelli and R. H. G. A. Kiminami, *J. Magn. Magn. Mater.*, 2003, **256**, 174-182.

[25] X. B. Zhou, L. Shen, L. Li, T. M. Huang, C. F. Hu, W. M. Pan, ... and Q. Huang, *J. Phys D. Appl. Phys.*, 2013, **46**, 145002.

[26] E. Açıkalın, O. Atıcı, A. Sayıntı, K. Çoban and H. Erkalfa, *Prog. Org. Coat.*, 2013, **76**, 972-978.

[27] Q. Li, Y. Li, X. Li, S. Chen, S. Zhang, J. Wang and C. Hou, *J. Alloy. Compd.*, 2014, **608**, 35-43.

[28] F. Yan, J. Li, J. Zhang, F. Liu and W. Yang, *J. Nanopart. Res.*, 2009, **11**, 289-296.

[29] A. T. Raghavender, N. Biliškov and Ž. Skoko, *Mater. Lett.*, 2011, **65**, 677-680.

[30] W. Han, *Polym. Composite.*, 2013, **34**, 156-163.

[31] L. Wang, Y. Shen, X. Lai and Z. Li, *J. Appl. Polym. Sci.*, 2011, **119**, 3521-3530.

[32] H. C. Kuan, W. P. Chuang, C. C. M. Ma, C. L. Chiang and H. L. Wu, *J. Mater. Sci.*, 2005, **40**, 179-185.

[33] Y. Yi, F. Ye, C. Huang and J. Guan, *J. Appl. Polym. Sci.*, 2010, **115**, 451-459.

[34] S. Zhang, Y. Li, L. Peng, Q. Li, S. Chen and K. Hou, *Compos. Part A: Appl. Sci. Manufac.*, 2013, **55**, 94-101.

RSC Advances Accepted Manuscript

[35] S. Chen, S. Zhang, Y. Li, G. Zhao, *RSC Adv.*, 2015, **5**, 4355-4363.

[36] Z. Huang and F. Tang, *J. Colloid. In. Terf. Sci.*, 2004, **275**, 142-147.

[37] J. O. Park, K. Y. Rhee and S. J. Park, *Appl. Surf. Sci.*, 2010, **256**, 6945-6950.

[38] M. Ashjari, A. R. Mahdavian, N. G. Ebrahimi and Y. Mosleh, *J. Magn. Magn. Mater.*, 2010, **20**, 213-219.

Figure captions:

Fig. 1 The brief synthesis process of WPU/h-NZFO nanocomposite.

Fig. 2 TEM image of pristine h-NZFO (a) and SEM micrographs of cross-section of pure WPU (b), WPU/pristine h-NZFO-4 (c), WPU/h-NZFO-4 (d), WPU/h-NZFO-6 (e) and WPU/h-NZFO-8 (f).

Fig. 3 The XRD patterns of h-NZFO (a), h-NZFO-NCO (b), pure WPU (c) and WPU/h-NZFO-4 nanocomposite (d).

Fig. 4 FT-IR spectra of h-NZFO (a), h-NZFO-NCO (b), pure WPU (c) and WPU/h-NZFO-4 nanocomposite (d).

Fig. 5 The particle size and size distribution of pure WPU (a) and WPU/h-NZFO-4 emulsions (b).

Fig. 6 The TEM images of pure WPU emulsion (a) and WPU/h-NZFO-4 emulsion (b).

Fig. 7 TGA curves of pure WPU (a) and WPU/h-NZFO nanocomposites with h-NZFO-NCO content is: 2% (b), 4% (c), 6% (d) and 8% (e).

Fig. 8 DMA loss factor curves of pure WPU (a) and WPU/h-NZFO nanocomposites

RSC Advances Accepted Manuscript

with h-NZFO-NCO content is: 2% (b), 4% (c), 6% (d) and 8% (e).

Fig. 9 DMA storage modulus curves of pure WPU (a) and WPU/h-NZFO nanocomposites with h-NZFO-NCO content is: 2% (b), 4% (c), 6% (d) and 8% (e).

Fig. 10 The emulsion images of WPU/h-NZFO-4 after placing for one month (a) and WPU/pristine h-NZFO-4 after placing for less than half an hour (b).

Fig. 11 The images of nanocomposite films of WPU/h-NZFO-4 (a) and WPU/pristine h-NZFO-4 (b) after UV-curing for 4 min.

Fig. 12 The SEM micrographs of upper surface (a), lower surface (b) of WPU/h-NZFO-4, upper surface (c) and lower surface (d) of WPU/pristine h-NZFO-4.

Fig. 13 Hysteresis loops of h-NZFO and h-NZFO-NCO (a) WPU/h-NZFO nanocomposites with different h-NZFO-NCO content (b).

Table 1.

The stability of WPU/h-NZFO emulsions with different h-NZFO-NCO content

h-NZFO-NCO content (%)	2	4	6	8	2 (pristine h-NZFO)
Stable time	>30 days	>30days	>24 days	>19 days	< 0.5 h

RSC Advances Accepted Manuscript

Table 2.

Mechanical properties of WPU and WPU/h-NZFO nanocomposites

h-NZFO content (wt.%)	Young's modulus/MPa	Tensile strength/MPa	Elongation at break(%)
0	218.4	17.5	386.6
2	212.3	15.7	340.3
4	203.7	19.5	279.6
6	165.6	12.1	239.5
8	132.2	9.9	228.1

RSC Advances Accepted Manuscript

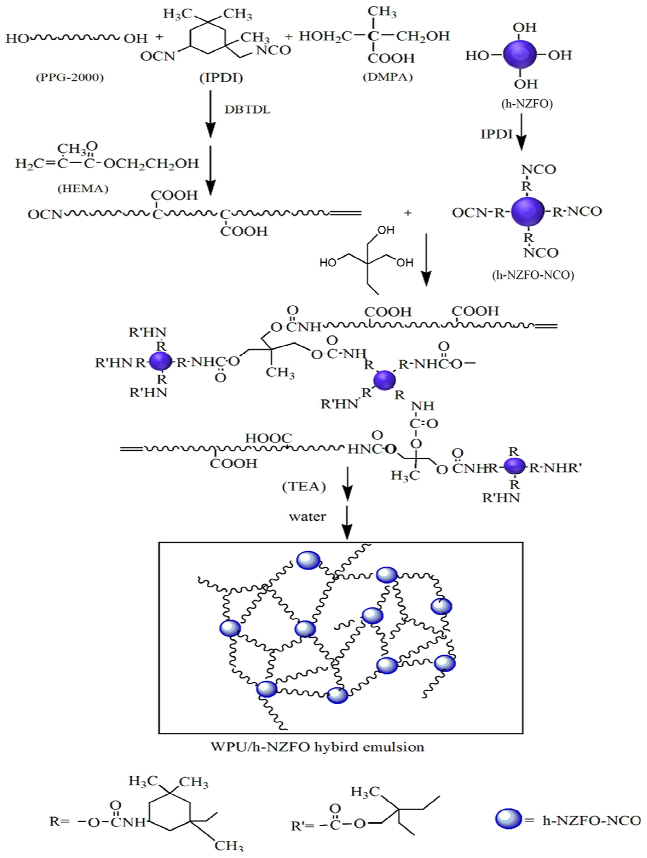

Fig. 1 The brief synthesis process of WPU/h-NZFO nanocomposite.

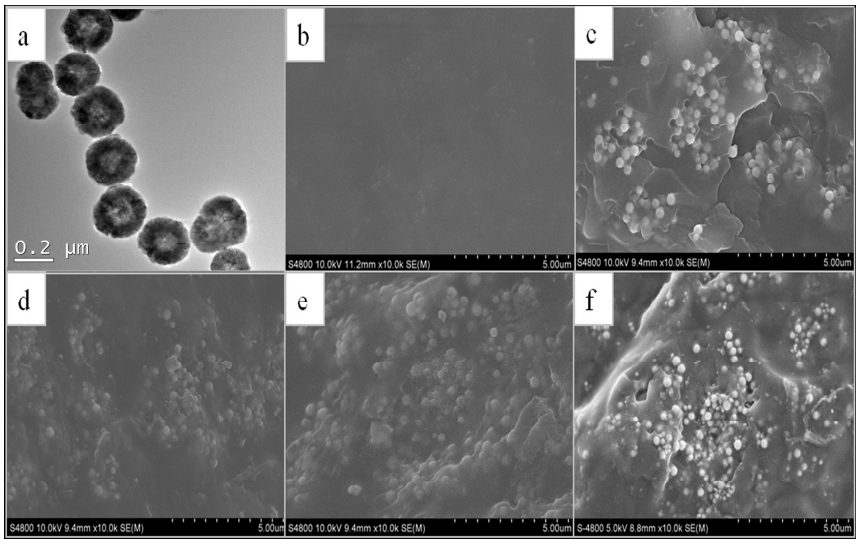

Fig. 2 TEM image of pristine h-NZFO (a) and SEM micrographs of cross-section of pure WPU (b), WPU/pristine h-NZFO-4 (c), WPU/h-NZFO-4 (d), WPU/h-NZFO-6 (e) and WPU/h-NZFO-8 (f).

RSC Advances Accepted Manuscript

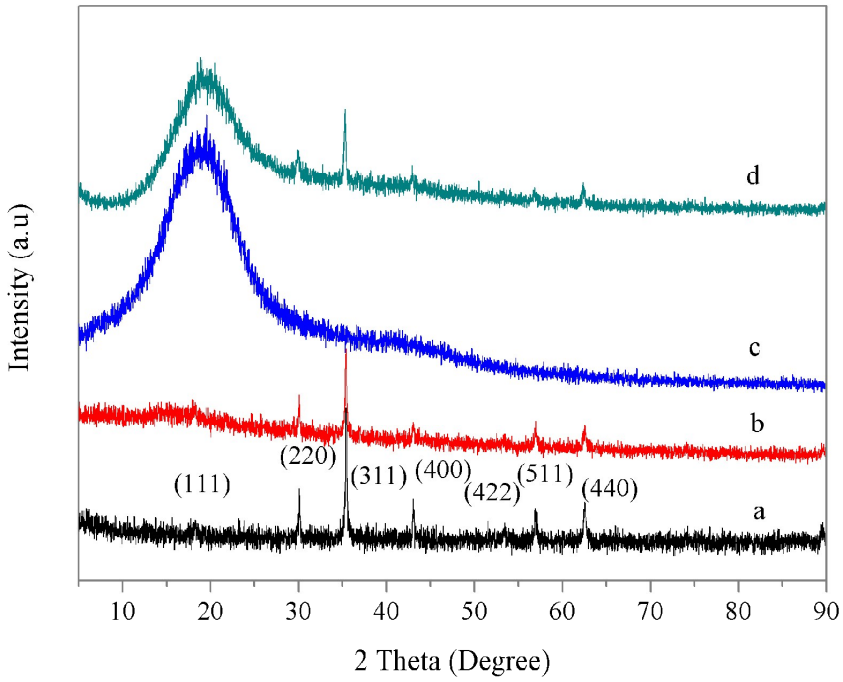

Fig. 3 The XRD patterns of h-NZFO (a), h-NZFO-NCO (b), pure WPU (c) and WPU/h-NZFO-4 nanocomposite (d).

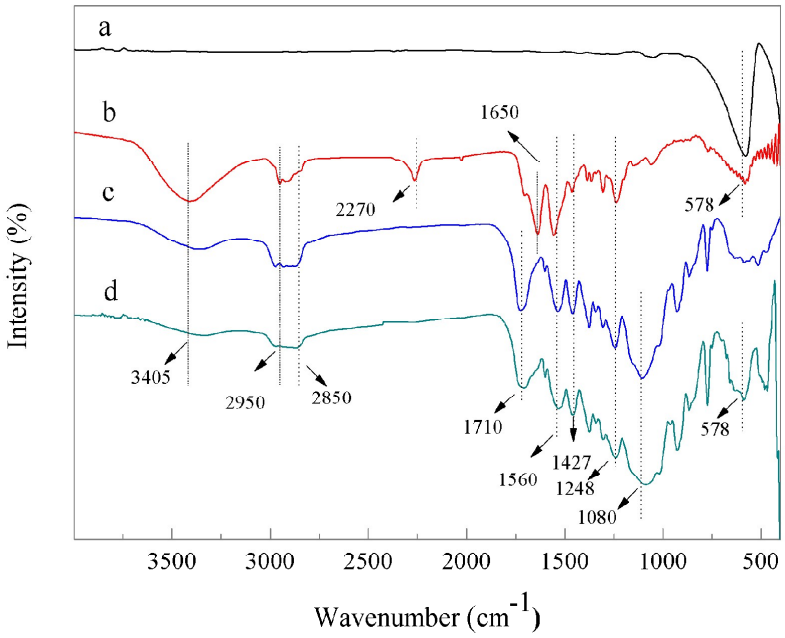

Fig. 4 FT-IR spectra of h-NZFO (a), h-NZFO-NCO (b), pure WPU (c) and WPU/h-NZFO-4 nanocomposite (d).

RSC Advances Accepted Manuscript

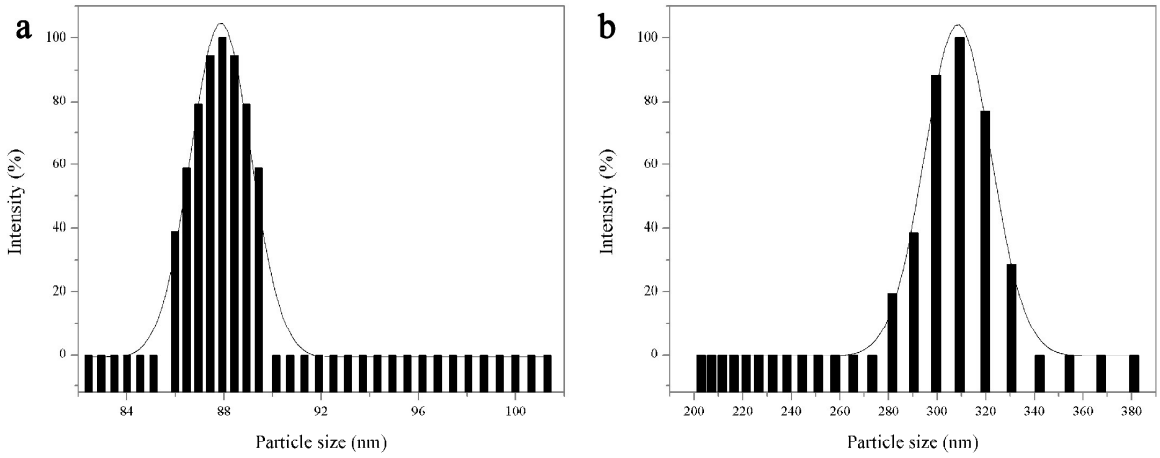

Fig. 5 The particle size and size distribution of pure WPU emulsion (a) and WPU/h-NZFO-4 emulsion (b).

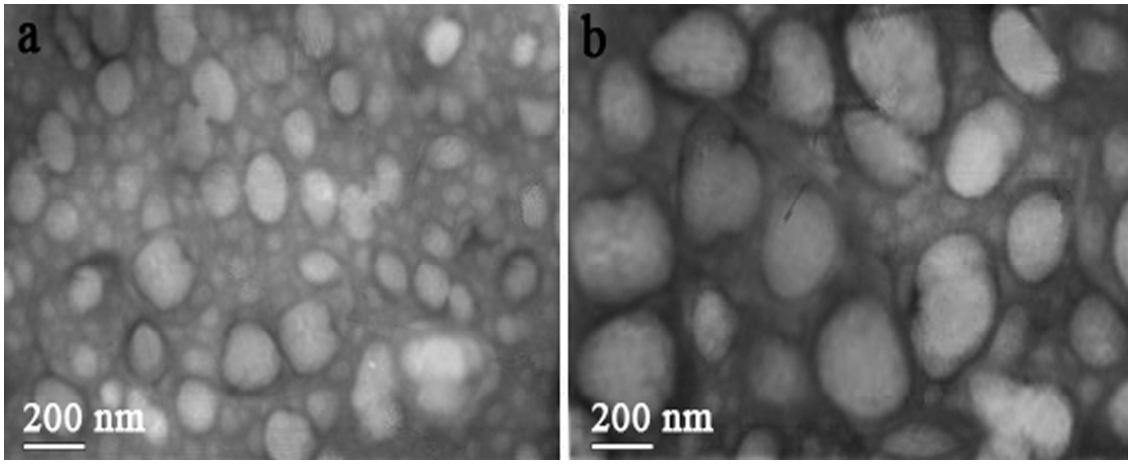

Fig. 6 The TEM images of pure WPU emulsion (a) and WPU/h-NZFO-4 emulsion (b).

RSC Advances Accepted Manuscript

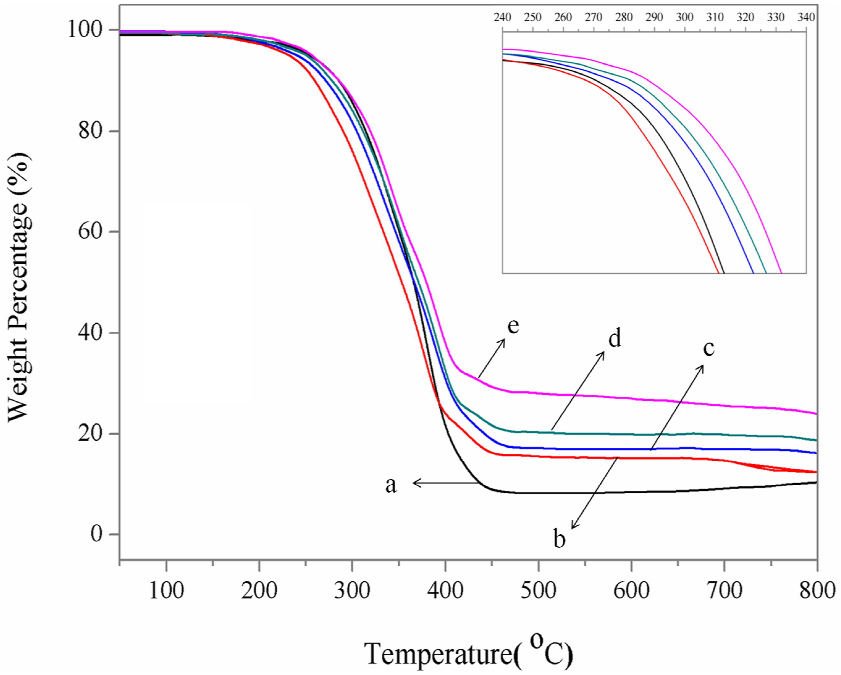

Fig. 7 TGA curves of pure WPU (a) and WPU/h-NZFO nanocomposites with h-NZFO-NCO content is: 2% (b), 4% (c), 6% (d) and 8% (e).

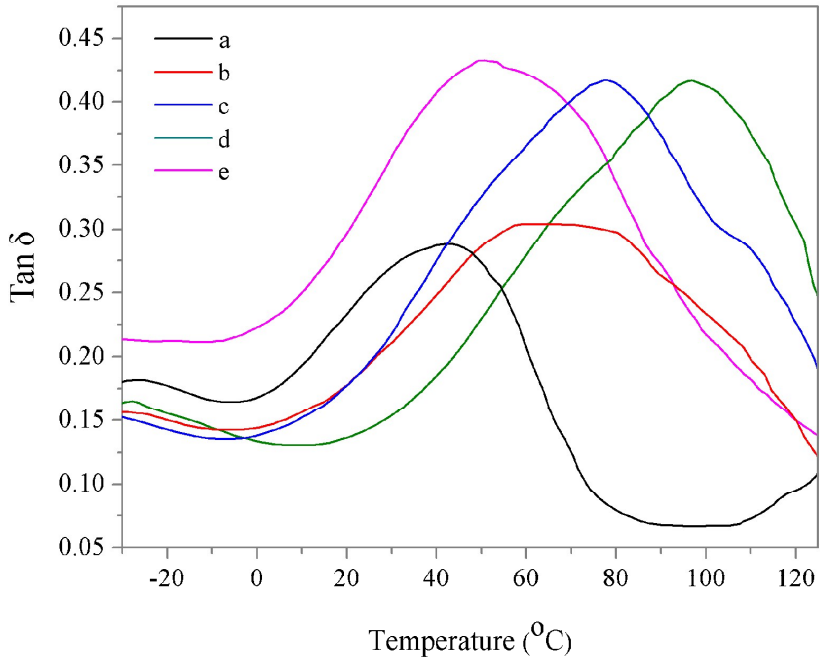

Fig. 8 DMA loss factor curves of pure WPU (a) and WPU/h-NZFO nanocomposites with h-NZFO-NCO content is: 2% (b), 4% (c), 6% (d) and 8% (e).

RSC Advances Accepted Manuscript

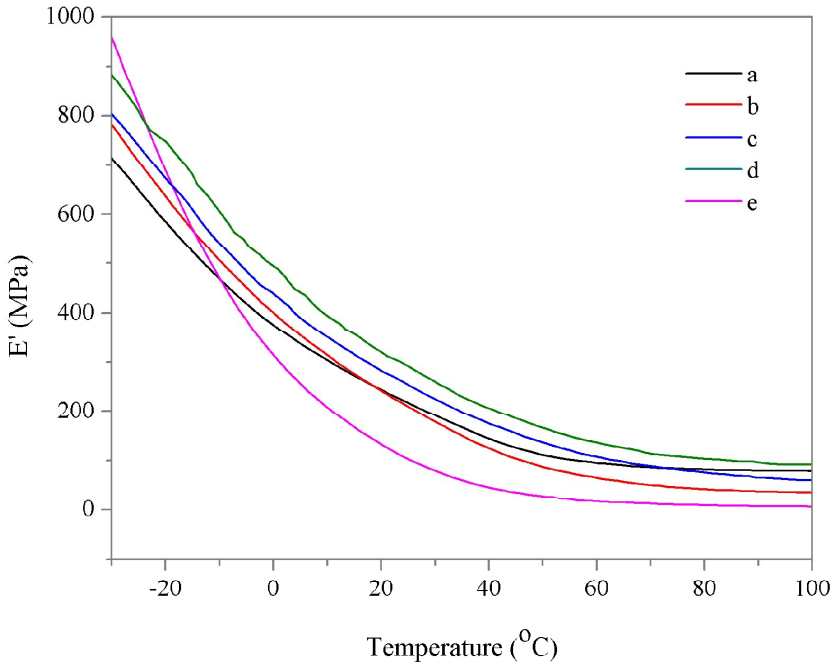

Fig. 9 DMA storage modulus curves of pure WPU (a) and WPU/h-NZFO nanocomposites with h-NZFO-NCO content is: 2% (b), 4% (c), 6% (d) and 8% (e).

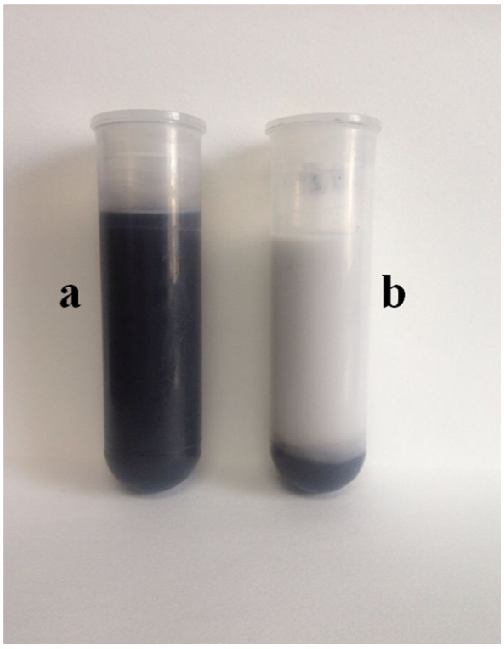

Fig. 10 The emulsion images of WPU/h-NZFO-4 after placing for one month (a) and WPU/pristine h-NZFO-4 after placing for less than half an hour (b).

RSC Advances Accepted Manuscript

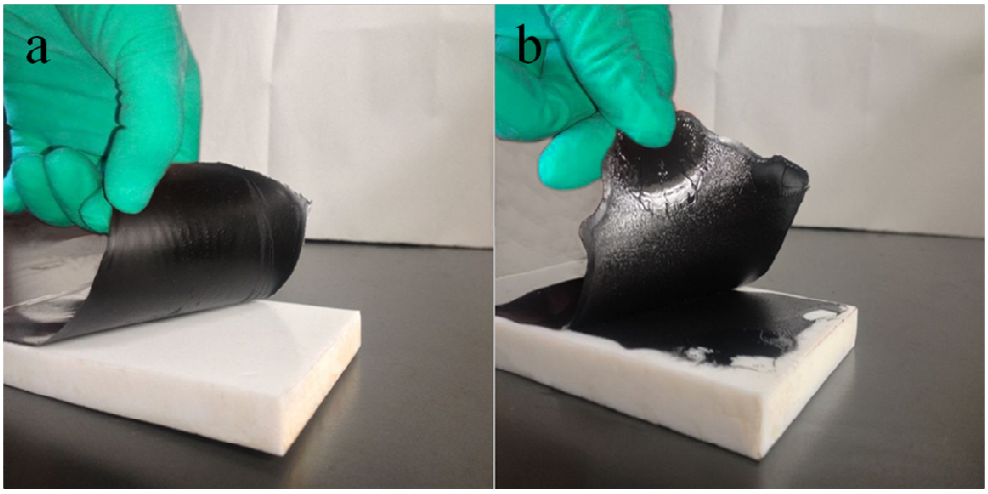

Fig. 11 The images of nanocomposite films of WPU/h-NZFO-4 (a) and WPU/pristine h-NZFO-4 (b) after UV-curing for 4 min.

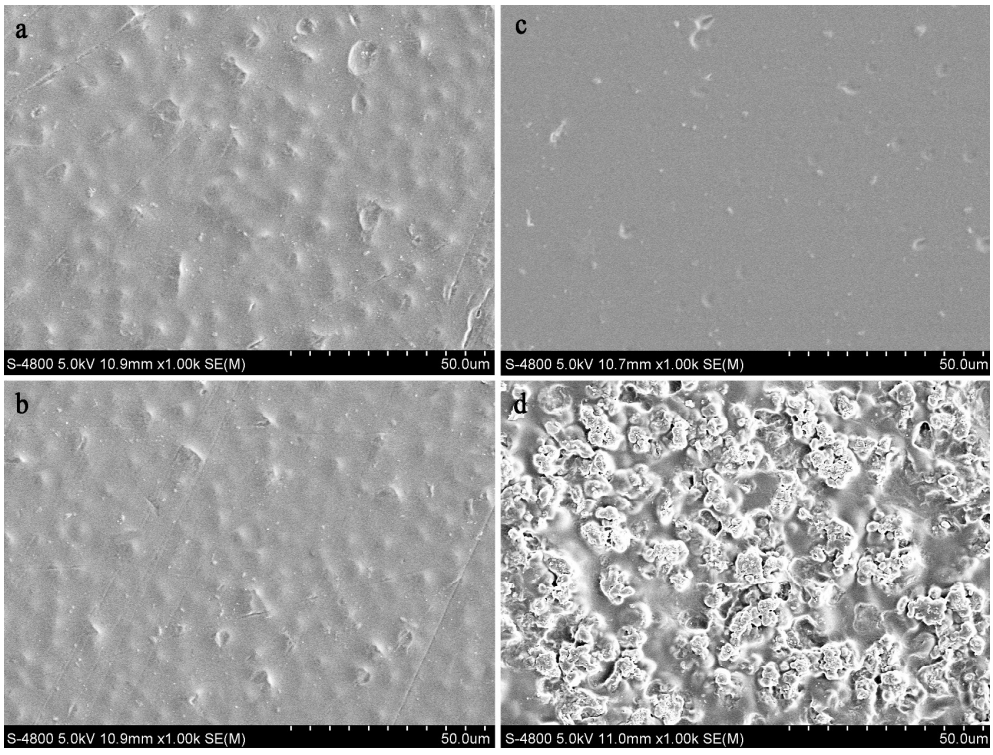

Fig. 12 The SEM micrographs of upper surface (a), lower surface (b) of WPU/h-NZFO-4, upper surface (c) and lower surface (d) of WPU/pristine h-NZFO-4

RSC Advances Accepted Manuscript

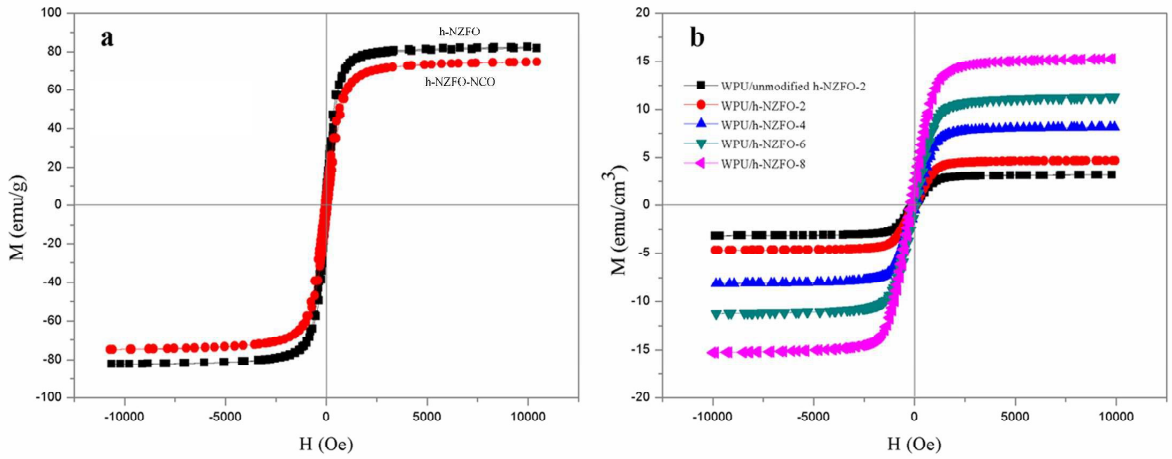

Fig. 13 Hysteresis loops of h-NZFO and h-NZFO-NCO (a) WPU/h-NZFO nanocomposites with different h-NZFO-NCO content.

RSC Advances Accepted Manuscript